Reconstructing Human Joint Motion with Computational Fabrics

RUIBO LIU, Department of Computer Science, Dartmouth College
QIJIA SHAO, Department of Computer Science, Dartmouth College
SIQI WANG, Department of Computer Science, Shanghai Jiao Tong University
CHRISTINA RU, Department of Computer Science, Dartmouth College
DEVIN BALKCOM, Department of Computer Science, Dartmouth College
XIA ZHOU, Department of Computer Science, Dartmouth College

Accurate and continuous monitoring of joint rotational motion is crucial for a wide range of applications such as physical rehabilitation [6, 85] and motion training [22, 54, 68]. Existing motion capture systems, however, either need instrumentation of the environment, or fail to track arbitrary joint motion, or impose wearing discomfort by requiring rigid electrical sensors right around the joint area. This work studies the use of everyday fabrics as a flexible and soft sensing medium to monitor joint angular motion accurately and reliably. Specifically we focus on the primary use of conductive stretchable fabrics to sense the skin deformation during joint motion and infer the joint rotational angle. We tackle challenges of fabric sensing originated by the inherent properties of elastic materials by leveraging two types of sensing fabric and characterizing their properties based on models in material science. We apply models from bio-mechanics to infer joint angles and propose the use of dual strain sensing to enhance sensing robustness against user diversity and fabric position offsets. We fabricate prototypes using off-the-shelf fabrics and micro-controller. Experiments with ten participants show 9.69° median angular error in tracking joint angle and its sensing robustness across various users and activities.

CCS Concepts: • **Human-centered computing → Ubiquitous and mobile computing systems and tools**; **Ambient intelligence**.

Additional Key Words and Phrases: smart fabric/textile, fabric/textile sensing, joint motion sensing

ACM Reference Format:
Ruibo Liu, Qijia Shao, Siqi Wang, Christina Ru, Devin Balkcom, and Xia Zhou. 2019. Reconstructing Human Joint Motion with Computational Fabrics. *Proc. ACM Interact. Mob. Wearable Ubiquitous Technol.* 3, 1, Article 19 (March 2019), 26 pages. https://doi.org/10.1145/3314406

1 INTRODUCTION

Human body joints are essential for actuating body motion. Accurate and continuous monitoring of their rotational movement is critical for physical rehabilitation [6, 85], motion training/coaching [22, 54, 68], sports analytics [48], human-robot or human-computer interactions [20, 47]. For rehabilitation patients with joint injuries or chronic joint pains, day-to-day measurement of joint's angular motion helps doctors assess the effectiveness of medical

Authors' addresses: Ruibo Liu, Department of Computer Science, Dartmouth College, 9 Maynard St, Hanover, NH, 03755, Ruibo.Liu.GR@dartmouth.edu; Qijia Shao, Department of Computer Science, Dartmouth College, Qijia.Shao.GR@dartmouth.edu; Siqi Wang, Department of Computer Science, Shanghai Jiao Tong University, siqi9794@sjtu.edu.cn; Christina Ru, Department of Computer Science, Dartmouth College, Christina.Ru.21@dartmouth.edu; Devin Balkcom, Department of Computer Science, Dartmouth College, Devin.Balkcom@dartmouth.edu; Xia Zhou, Department of Computer Science, Dartmouth College, Xia.Zhou@dartmouth.edu.

2474-9567/2019/3-ART19 $15.00
https://doi.org/10.1145/3314406

and physical treatments, since joint and muscle repair takes long enough that it is impractical for expert therapists to remain with patients at all times; for students learning precise motions from instructors in the educational context (e.g., athletic coaching, yoga training, learning a complex surgical procedure), monitoring joint angles allows instructors to analyze detailed joint movements and provide fine-grained corrections and feedback.

All these applications demand joint motion sensing systems that are portable, comfortable for long-time wear, and capable of sensing subtle motion. Existing technologies for motion capture, however, still fall short in meeting these requirements. High-end systems such as VICON [87] or Kinect require heavy instrumentation of the environment (e.g., setting up multiple infrared cameras). More portable systems either achieve coarse sensing granularity by classifying a limited set of gestures/poses and thus cannot track arbitrary motion, or require users to constantly wear rigid electrical sensors right around the joint area [18, 75, 91], where such placement inflexibility often causes the system burdensome to wear.

In this work we consider the use of everyday fabrics as an unobtrusive sensing medium to continuously and accurately monitor joint angular motion. Requiring neither infrastructure support nor rigid electrical sensors on the joint, our approach relies on fabrics/textile *alone*, as a soft and natural sensing layer around joints, to reconstruct the angles of body joints at a fine granularity. While the concept of e-textile has been proposed in prior studies for various applications, prior works either offer coarse sensing capabilities [49, 58, 62, 82] or still require embedding electronics into textiles by using textile as a substrate for attachment of sensors. We aim to advance the state-of-the-art by achieving qualitative advances in sensing capability and reliability, and more importantly, by focusing on the use of off-the-shelf, low-cost (e.g., $50) fabrics alone for motion sensing without extra electrical sensors. Such a minimalist sensing approach renders the sensing system comfortable to wear, low-power, and low-cost.

Specifically, we study primarily the use of conductive stretchable fabrics with knitted structures. As shown in Figure 2(b), a knitted fabric is constructed by a continuous loop of yarns. Made of conductive stretchable threads, the knitted fabric reacts to different levels of strain with varying resistance. The change in resistance is caused by alterations of the yarns' contact points and contact pressure under tension [32]. This property can be exploited to sense body joint motion, where we wrap a joint with conductive stretchable fabrics (also serving as a joint protective wrap commonly worn during exercises for joint protection). Joint rotation and muscle movement cause skin deformation and thus strain of the fabric. By continuously monitoring the fabric's resistance, we can infer the muscle strain caused by the current joint motion, and thus recover the joint angle. The system only requires a micro-controller fetching data on fabric resistance through conductive threads. The micro-controller can be placed away from the joint for greater comfort flexibility. As an example, it can be embedded into a button to hide its appearance and it can be easily detached when necessary.

To realize this conceptually simple idea as a practical system providing accurate and robust motion sensing, we are confronted with several challenges. *First*, with off-the-shelf stretchable fabrics, the resistance change and the level of strain do not exhibit a one-to-one mapping, and even worse, their relationship depends on the type of motion (e.g., flexion/loading or extension/unloading), caused by the *hysteresis* intrinsic to elastic materials. It results in ambiguities in inferring skin deformation solely based on the observed changes in fabric resistance. *Second*, fabric as a strain sensor does not provide a stable output even under a constant strain. This is a phenomenon common in stretchable materials and referred to as the *stress relaxation* in material science. Such relaxation further increases the ambiguity in inferring skin deformation and leads to errors that accumulate over time. *Third*, even with perfect derivation of skin deformation, inferring the actual joint angle is still nontrivial. For one, bone shape and soft tissue distribution differ significantly across users. Additionally, joint motion can lead to the sensing fabrics sliding subtly around the joint. Both individual differences and the motion artifact of the sensing fabrics pose challenges in achieving robust motion sensing in practice.

We address the above challenges as follows. To disambiguate motion states, we add a small piece of pressure fabric to augment the primary sensing fabric (i.e., strain sensors). The pressure fabric senses the pressure from

the joint to the fabric during motions. Although it alone cannot provide precise sensing of subtle motion, it can steadily differentiate coarse motion states: flexion, extension, or the motionless state. We characterize the strain fabric's resistance change in different motion states, and apply models from material sciences to compensate for the stress relaxation during the motionless state. Finally, we leverage models in the literature of bio-mechanics to characterize the geometric relationship between skin deformation and joint angle. To deal with individual differences and motion artifact of the sensing fabrics, we place two straps of strain fabrics as dual sensors above the joint. We consider the differences of the stretch lengths of these two strain fabrics, which cancel out the impact of the body part thickness or slight offset of fabric positions.

Using the elbow joint as an example, we fabricate prototypes in two sizes (27/20.5 cm lower-elbow perimeter, 31/23 cm upper-elbow perimeter) using off-the-shelf fabrics and micro-controller (Adafruit Flora). We place strain fabrics and pressure fabrics in separate layers to enhance their sensing resilience and sensitivity. Inelastic fabrics are used as reference resistor for the micro-controller to monitor the resistance change of strain and pressure fabrics, where micro-controller and sensing fabrics are connected via conductive threads. we test our prototypes with ten participants to examine sensing accuracy and robustness. We also seek participants' feedback on the wearing comfort. We summarize our key findings as below:

- The system reconstructs elbow joint angles with a median error of 9.69° across users with different arm sizes, under motions with various speeds and magnitudes;
- The sensing performance is robust against slight displacement (up to 1 cm) of the sensing fabrics around the joint, and the system allows gentle hand wash with minor degradation (7.64°) in sensing accuracy after wash;
- Participants generally rate the prototypes comfortable to wear and flexible to adapt to various motions.

2 BACKGROUND ON FABRIC SENSING

Fabric as a sensor presents numerous benefits, as it is soft, light, flexible, and thus easy to wear even during exercises. In particular, our study considers off-the-shelf stretchable textile made of conductive threads as our primary sensing fabric. The sensing ability of such fabrics stems from their knitted micro-structures of the yarns, where an external strain causes changes in the number of contact points and contact pressure, resulting into changes in the contact resistance of the fabric [12, 32, 64, 80]. We next experimentally examine the property of such fabrics and their sensing capability.

Experimental Validation. We test an off-the-shelf stretchable conductive fabric (LessEMF #A321) [34]. With 76% Nylon and 24% elastic fiber, it can be stretched by up to 100% along its length/course direction and 60% along its width/wale direction. Its yarns are plated with a thin silver layer offering great conductivity. We cascade the test fabric with a fixed-value reference resistance. We use a micro-controller to measure the voltage on the test fabric to monitor its resistance change under various levels of strain. To systematically apply various levels of strain, we use a professional tensile test machine (Instron 4442). Figure 1 illustrates the overall setup. We evaluate fabric's resistance change via the metric of *resistance change ratio* $r_{\Delta R} = (R_2 - R_1)/R_1$, where R_1 and R_2 denote the original and current resistance, respectively. With the original voltage as U_1 and current voltage as U_2, $r_{\Delta R}$ can be computed as:

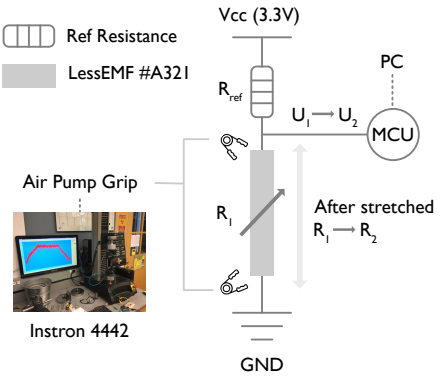

Fig. 1. Test platform configuration

$$r_{\Delta R} = \frac{R_2 - R_1}{R_1} = \frac{V_{cc}U_2 - U_1U_2}{V_{cc}U_1 - U_1U_2} - 1, \tag{1}$$

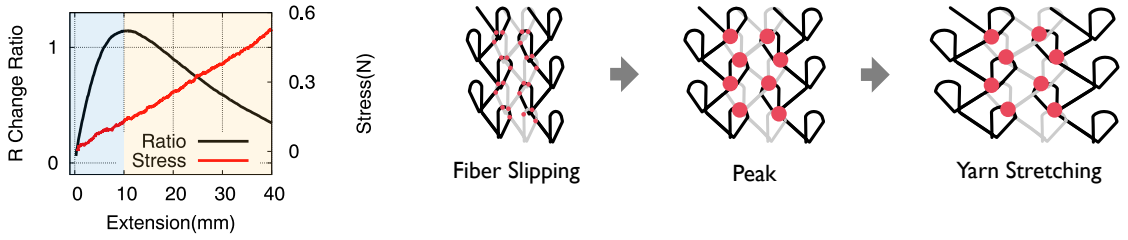

(a) Overall trend (b) Various phases during a stretch

Fig. 2. The change of fabric resistance as the fabric is stretched. Resistance sharply increases due to the decrease in yarn contact points during fiber slipping, and then gradually decreases under increasing contact pressure during yarn stretching.

where V_{cc} is the power supply voltage from the micro-controller.

Figure 2(a) plots the resistance change ratio as a 15 cm × 3 cm fabric is stretched along its course direction. We also plot the stress on the fabric recorded by Instron. We obtain two main observations. *First*, the fabric is very sensitive to motion, where even millimeter-level stretches cause noticeable changes in resistance (e.g., 2cm stretch leads to 60% resistance change). It provides basis for sensing fine-grained motion. *Second*, as the strain grows, the change in fabric resistance is not monotonic; rather, it undergoes a sharp increase, followed by a gradual decline. We observe similar patterns consistently across various test runs and across other types of stretchable fabrics we have tested. This pattern can be explained by examining how contact points and contact pressure are altered under strain. Based on the Holm's theory [32], the contact resistance of a conductive fabric is inversely proportional to the number of contact points and the contact pressure. In the beginning when the fabric is being slightly stretched, the stress on the fabric is not evident and the change in the number of contact points dominates the resistance change. The low level of strain only causes fiber slipping within air gaps and forming tighter block structure. As a result, the number of contact points decreases, leading to an increase in contact resistance. As the fabric is further stretched under higher levels of strain, the stress on the fabric becomes the dominant factor that changes the resistance. Since there is no more space for yarns to form blocks, the number of contact points stays constant. The growing inner stress among yarns leads to the decline of the contact resistance. Figure 2(b) illustrates fabric's micro-structure during different phases of the process.

We further test the resistance change as we stretch the fabric in the wale direction. We cut two pieces of fabrics in the same size (15cm × 3cm), one with course direction along its length and the other with wale direction along its length. We stretch both fabrics to 30% of its original length and plot the resistance change ratios in Figure 3(a). We observe that resistance change exhibits a similar trend yet with distinct details: stretch in the course direction leads to more significant changes in resistance (over 100%), while that in the wale direction leads to only around 5% change in the resistance. Figure 3(b) and 3(c) show the microscope images of each fabric under 30% strain.

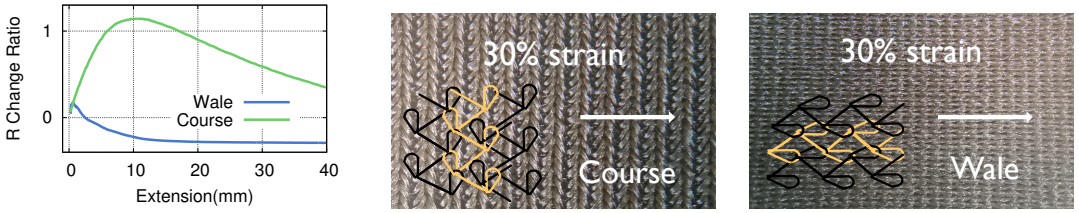

(a) Impact of stretch direction (b) 30% strain in the course direction (c) 30% strain in the wale direction

Fig. 3. Resistance change of stretchable conductive fabric when it is stretched along its wale or course direction (a). (b) and (c) are microscope images on fabric's micro-structure under 30% strain along the course and wale direction, respectively.

We also examine the impact of fabric's size ratio on its sensitivity to strain. Figure 4 compares various fabrics in various size configurations when they are stretched in the course direction. We observe that increases in the width result into higher peaks, because more yarn blocks are formed, leading to fewer contact points and larger increase in resistance. On the other hand, under a fixed width, longer fabrics have more air gaps in the stretching direction and thus need more strain to reach the peak, leading to the peak occurred under larger stretch lengths. Additionally, we observe that a thinner fabric (1-cm width) has more high-frequency noise in its signal response. We hypothesize that the thinner fabric has weaker fiber strength, making it harder to keep a stable structure and stable resistance value. Overall, wider and longer fabrics are more preferable for sensing purposes.

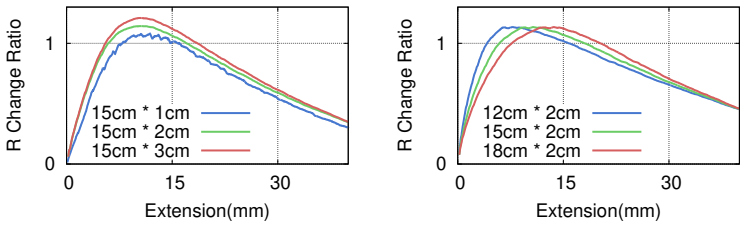

(a) Varying width (b) Varying length

Fig. 4. Impact of fabric size configuration on its sensitivity to stretch.

Summary. Our experiments results validate that off-the-shelf stretchable conductive fabrics are sensitive to motion when they are stretched along the course direction. Even millimeter-level stretches lead to noticeable changes in resistance, providing basis for the fabric to sense skin deformation caused by subtle joint motion. Under increasing strain, the change in fabric's resistance is non-monotonic, starting with a sharp increase followed by a gradual decline. Wider and longer fabrics provide more stable, substantial change in resistance under strain.

3 CHALLENGES IN FABRIC SENSING

While prior results are promising, fabric as a sensor also presents numerous challenges, especially for the purpose of accurately and robustly inferring joint angles. We elaborate on the challenges as follows.

Elastic Hysteresis. The non-monotonic nature of the fabric resistance change under increasing strain indicates that there is no one-to-one mapping between the observed resistance change and the stretch length. Compounding this problem is the fact that the characterization of the resistance change also depends on the type of motion. When the fabric is being extended under strain (loading), its resistance change follows a curve that is different from that when the fabric is retracting as the strain is reduced (unloading). The difference is due to the en ergy dissipation caused by material internal friction. This phenomenon is referred to as *hysteresis*, an intrinsic property of elastic materials. As an example, Figure 5 plots the ratio of resistance change during loading and unloading, with the LessEMF fabric (15.3cm × 3cm in size). It implies that an observed value of resistance change can correspond to up to four possible stretch lengths, making it hard to uniquely infer the current skin deformation.

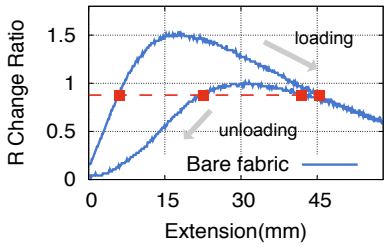

Fig. 5. Elastic hysteresis. Resistance change follows a different curve during loading/extending and unloading/retracting.

Instability. Furthermore, our experiments reveal that the impact of strain on fabric's resistance change slightly varies across repeated rounds of stretching. Thus, it is difficult to characterize the mapping between resistance change and extension length using a single function with fixed parameters. To examine this instability, we stretch a 15 cm × 1.5 cm fabric to 30% of its original length along the wale direction and repeat it for 160 rounds. Figure 6(a) plots the resistance change ratio as the extension length increases. We observe that curves from different rounds

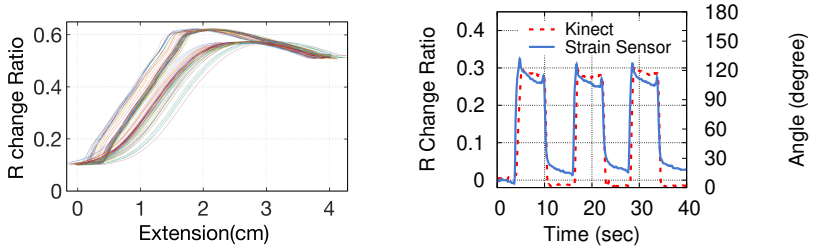

(a) Instability of resistance change (b) Stress relaxation

Fig. 6. The impact of stress relaxation (a) and the instability of resistance change in 160 rounds of stretching (b).

do not exactly overlap and exhibit slight offsets. As suggested in [37], a dominant factor causing these offsets is electromagnetic (EM) coupling with ambient electromagnetic interference. Here each conductive thread of the fabric is similar to an antenna and the large number of threads can easily absorb ambient electromagnetic noise, affecting how fabric's resistance changes under strain.

Stress Relaxation. Another challenge comes from the fact that fabric resistance does not stay at a stable value under a constant strain. This is known as *stress relaxation* in the literature of material science, a property commonly seen in elastic polymer because of the loose connection of its fiber [39, 74]. Figure 6(b) plots the resistance change ratio as a LessEMF fabric (15 cm × 1.5 cm in size) is stretched three times by the Instron tensile machine, where each time the strain is kept constant for 60 seconds. We observe that the resistance slowly drops by 12% after 5 seconds under a constant strain. Such instability brings more ambiguities in deriving a single deformation/stretch value based on the observed resistance change.

User Diversity and Motion Artifact. Finally, inferring the actual joint angle based on the sensed deformation on the skin is challenging given the differences of body parameters and motion patterns across users. This has been confirmed as one of the main sources of error in designing wearable systems in prior works [15, 30]. Specifically in our context, the relationship between the joint angle and the skin surface deformation depends on the bone shape and soft tissue distribution. Additionally, sensing fabrics can slightly slide during joint motions. As a result, the stretchable fabric can end up measuring skin deformation at various spots during the course of a motion, and the measurement inconsistency can hurt sensing accuracy. To address such motion artifact, prior works have considered applying a calibration in the beginning of each wearing [17, 19, 25, 41, 78], or the use of sensor array with machine learning algorithms [14, 31, 49, 52]. These methods, however, can handle only the initial offset caused by wearing, not the error during the motion. We aim to seek solutions that are robust against slight position offsets of the sensing fabrics during joint motions.

4 SYSTEM DESIGN

We address above challenges via four key design elements:

- **Augmentation with Pressure Fabric**: To tackle the lack of one-to-one mapping between stretch length and resistance change, we augment strain fabrics with collocated pressure fabrics. Sensing the pressure from the joint motion, pressure fabrics are less sensitive to subtle joint motion and exhibit a narrower sensing range. However, they offer robust differentiation of coarse motion states (loading/extending, unloading/retracting, motionless). Once the motion state is identified, the system can select the proper modeling on strain fabric's resistance change for inferring the actual skin deformation.
- **Gaussian Distribution Curve**: Instead of relying on a single function to characterize the resistance change ratio under varying stretch length, we study the *distribution* of resistance change ratios to address the instability

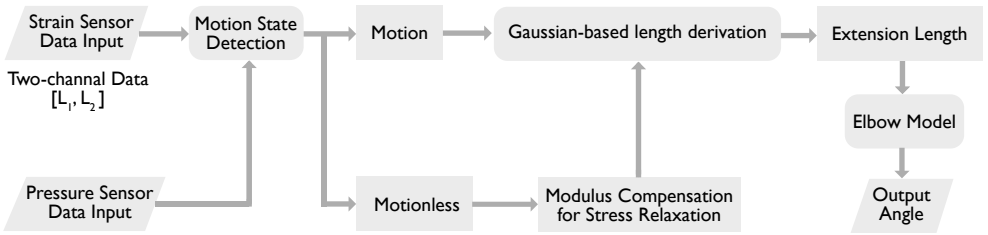

Fig. 7. System design overview.

problem. Applying a statistical graphical method (Quantile-Quantile plot), we validate that the distribution is Gaussian. We then design a probability-based method to infer the extension length.

- **Modeling Stress Relaxation**: we model fabric's stress relaxation by leveraging the literature from material science. We first apply the classical spring-dashpot model [33, 66] to characterize fabric's resistance change. We then model the stress relaxation via a relaxation modulus and use the model to compensate for the resistance decline during stress relaxation.
- **Dual Strain Fabrics for Inferring Joint Angle**: we derive the geometric relationship between skin deformation and joint rotational angle based on the anatomy of joints in biomechanics. We propose the use of two parallel strain fabrics separated with a fixed interval and examine the difference between the two fabrics to cancel out the impact of fabrics' motion artifact and robustly infer joint angle.

Figure 7 illustrates the overall system flow. We next describe each element in detail.

4.1 Augmentation with Pressure Fabric

Our first design element augments strain fabric sensing with pressure fabric to disambiguate motion states. Pressure is created by the squeezing of body joint and sensing fabrics. Pressure alone does not lead to precise sensing of joint motion. However, it can serve as an instructive reference to differentiate coarse motion states. We consider collocating strain fabrics and a small piece of pressure fabric (the actual placement is described in §5), so that they respond to the same joint motion and complement each other's sensing ability.

Characterization of Pressure Fabric. Pressure fabric commonly contains velostat, linqstat or other piezo-resistive materials whose resistance changes under pressure. Prior works have explored various layouts of such fabric, including grid [63], circle [88], and stripes [73]. Pressure fabric is known to exhibit poor resilience and random signal drift because of its unsatisfactory mechanical property of the dieletric polymer layer [42, 81]. Thus, it is not suitable for accurately sensing subtle motion. However, its superior binary distinguishable upper and lower bounds with its linear slope enables it to be qualified motion monitor. We place it on the top of the bulge formed by bending a joint, so that it differentiate coarse motion states such as flexion and extension.

We have tested various materials (velostat [72] vs. NW170-SLPA-2k by EeonTex [71]), number of layers, and material of electrodes (woven conductive fabric vs. NW170-PI-20 by EeonTex [70]) as the pressure fabric. The results of various configurations are shown in Figure 8. We observe that overall, resistance decreases when the fabric is pressed, leading to negative resistance change ratios. Resistance changes more significantly with more layers. Changing the conductive cover from NW170-PI-20 to woven conductive fabric results into noisier resistance values. The reason could be the porosity of woven fabric, which causes poor contact with the pressure sensitive material. NW170-SLPA-2k pressure sensitive fabric by EeonTex exhibits the smallest resistance change given the same level of pressure. Thus, we settle on the two-layer structure with velostat in the middle as the pressure-sensing material.

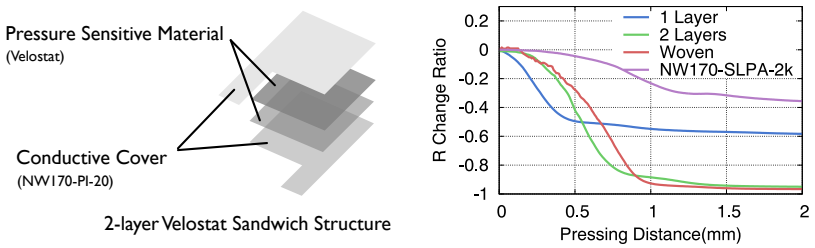

Fig. 8. Examining the resistance change of various pressure fabrics under pressure.

Disambiguating Motion States. Based on pressure fabric's resistance change, we aim to differentiate two motion states (*loading*, *unloading*) and a *motionless* state. Disambiguating these states is essential as each state corresponds to a different modeling of strain fabric's resistance change. Once a motion/motionless state is identified, the system can later apply the correct model on strain fabric's resistance change to derive the actual skin deformation (i.e., stretch length).

The differentiation of these motion states is based on the observation that joint flexion during loading raises the pressure sensed by the fabric (thus lowering the resistance), whereas joint extension during unloading lowers the pressure at the fabric (thus raising fabric resistance). Motionless states lead to relatively stable pressure at the fabric. Therefore, these motion/motionless states can be detected by examining the first-order derivatives of the pressure fabric's resistance change over time. A negative derivative indicates joint flexion/loading, while a positive derivative indicates joint extension/unloading. A derivative close to zero indicates motionless states.

Directly computing derivatives over pressure fabric's raw data, however, is prone to errors, given that sensor data are noisy and fluctuate over time. The noise can be introduced by the slight movement of the fabric over skin, or by the lack of sufficient force to the body [28, 55, 67]. To deal with sensor noises and ensure a robust detection, we smooth the raw data within a sliding window, interpolate data points between adjacent data points, and then compute the derivatives with the interpolated data points to obtain a more accurate trending of the raw data. Specifically, we use Gaussian kernel fitting, an algorithm whose core is the widely-used Gaussian kernel [83].

Algorithm 1 lists the detail in differentiating motion states, where $\hat{x}$ denotes interpolated data points. Data from pressure fabric are first fed into a circular buffer where the pointer to the data moves circularly, so that we can decrease the lag caused by real-time computation. Then we smooth the data in the buffer within a sliding window avoiding mutation in sequential data stream. Next, for the newly updated buffer, we interpolate data points based on the discrete data points in the buffer and then compute the first derivative with the interpolated data points. We compare the derivative k_t to a threshold k_{Motion} to determine if it is a motionless state. We then examine the sign of k_t to differentiate loading and unloading states. Figure 9 shows an example run of the algorithm, where 1 means loading, -1 denotes unloading, and 0 means motionless states. For motionless status, pressure fabric data are further compared with two pre-set thresholds to decide whether the state is motionless with strain or without strain. With the identified motion state, next we describe the modeling of strain fabric's resistance change to derive the stretch length (i.e., skin deformation).

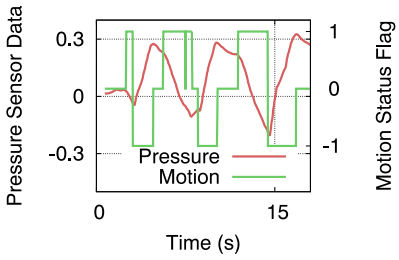

Fig. 9. Detection of motion states.

ALGORITHM 1: Detecting Motion States.

Input: Data from pressure fabric x_t.
Output: Motion state: loading, unloading or motionless.
repeat
  $Motion = Motionless$;
  insert new data into the circular buffer buf;
  for *each* buf *updated by new data* x_t **do**
    $\hat{x} \leftarrow$ data interpolation;
    Gaussian kernel ($\phi(\hat{x}, x_t) = exp\left(-\frac{(\hat{x}-x_t)^2}{2b^2}\right)$) regression on the buffer buf with kernel's input scale b;
    calculate the slope k_t of current curve at data point x_t;
    if $|k_t| < k_{Motion}$ **then**
      continue;
    else
      $k_t < 0 \rightarrow Motion = Loading$;
      $k_t > 0 \rightarrow Motion = UnLoading$;
    end
  end
until *no more data point comes in*;

4.2 Derivation of Stretch Length

The second design element aims to infer stretch length based on fabric's resistance change. Given the instability of resistance change across repeated stretch cycles, we examine the distribution of resistance change ratios under a given stretch length across different rounds of stretch. Based on the characteristics of the distribution, we design a probability-based method to infer the stretch length. We next describe our analysis of the distribution and the probability-based method in detail.

Distribution Analysis. Earlier results indicate that the same level of strain (i.e., stretch length) can lead to different resistance change ratios across repeated stretches (Figure 6(a)). We set out to analyze the distribution of resistance change ratios under a given stretch length. We stretch the fabric up to four centimeters 160 rounds on the tensile test machine while sampling fabric's resistance change ratio at 100 Hz. In total, we obtained 400 data points in each round and 160 data points (i.e., resistance change ratios) for each stretch length. At certain stretch length, we analyze the distribution of resistance change ratios. Using a statistical graphical method (Quantile-Quantile plot), our results reveal that the distribution is Gaussian. Quantile-Quantile (Q-Q) plot is a probability plot, which compares two probability distributions by plotting their quantiles against each other [86]. Here we fix one probability distribution as the standard Gaussian distribution and compare each distribution with it. Figure 10 shows an example. We observe that the points distribution is almost linear, suggesting that the distribution of resistance change ratios under a stretch length is Gaussian [29].

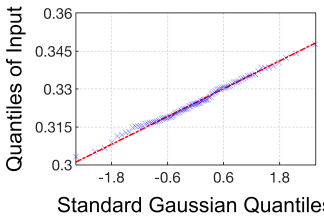

Fig. 10. Q-Q plot of sample data vs the standard Gaussian distribution.

Probability-Based Length Derivation. We exploit the Gaussian distribution of resistance change ratios for each stretch length to infer stretch length. Specifically, for each stretch length, we derive the mean and variance of the Gaussian distribution of resistance change ratios and store them in a look-up table. We then divide the look-up table to four classes, which are resistance increase during loading, resistance decrease during loading,

ALGORITHM 2: Extension length derivation.

Input: Data from strain fabric x_t and motion state ($Motion_1$): loading/unloading
Output: Extension length.
buf: circular buffer;
repeat
  insert new data into the circular buffer;
  for *each* buf *updated by new data* x_t **do**
    slope-based method → $Motion_2$ = increasing/decreasing
    Combine the $Motion_1$ and $Motion_2$ → MotionClass;
    for *each distribution in this class* **do**
      calculate the probability P_i
    end
    find the maximum probability P_{max};
    return the extension length corresponding to P_{max}.
  end
until *no more data point comes in*;

Table 1. Average MSE and RMSE of inferred extension based on leave-one-out cross-validation for strain sensor 1 and 2.

State	Strain Sensor 1		Strain Sensor 2	
	MSE	RMSE/cm	MSE	RMSE/cm
Loading_increase	0.0063	0.0792	0.0045	0.0674
Loading_decrease	0.0168	0.1292	0.0084	0.0918
Unloading_increase	0.0231	0.1518	0.0211	0.1452
unloading_decrease	0.0204	0.1428	0.0046	0.0676

resistance increase during unloading, and resistance decrease during unloading. Upon a sensed resistance change ratio, we first determine the class it belongs to based on the slope-based method and the output of pressure sensor. We then calculate its corresponding stretch length as well as probability based on each Gaussian distribution. The length with the maximal probability is selected as the inferred stretch length. Algorithm 2 lists the detailed steps.

Validation. To validate our length derivation algorithm, we use leave-one-out cross validation to evaluate its accuracy. In each fixed extension length, we have collected 160 resistance change ratios. We use 159 values to calculate the mean and variance of one particular Gaussian. For 400 stretch lengths (i.e., Gaussian distributions), we set the MotionClass of these 400 points and run Algorithm 2 to derive the stretch length. We calculate the mean squared error (MSE) and root mean squared error (RMSE) for each extension length. We summarize the results of two strain sensors in Table 1, respectively. We observe that the algorithm's RMSE for each motion class is around 0.1 cm, which demonstrates that our algorithm performs well in mapping the resistance change ratios to extension lengths.

4.3 Modulus Compensation for Stress Relaxation

The third design element aims to compensate for stress relaxation. With the second design element, we can derive the extension length in motion states. For motionless states where stress relaxation occurs, we apply relaxation model from the literature of material science to compensate for the impact of stress relaxation. Its core lies in the characterization of strain fabric's resistance change.

For most typical polymers whose conformational change is eventually limited by the network of entanglements or other types of junction points, a classical "spring-dashpot" model is effective to analyze its properties [33, 56, 66, 90]. Here, since we add an additional layer of elastic material parallel to the sensing material, we choose

Maxwell form (instead of Kelvin-Voigt form) standard linear solid model to describe our strain fabric [84]. As shown in Figure 11, the model consists of a spring-dashpot branch and another spring placed parallel with the branch. We mark the stiffness of the whole system and two springs as k, k_1, and k_2, respectively, while that of dashpot as η. We denote overall stress and the stress on each branch as σ, σ_1, and σ_2, respectively, and the deformation as ϵ, ϵ_1, and ϵ_2. Based on the physical properties of parallel springs, we obtain these relationships: $k = k_1 + k_2$, $\sigma = \sigma_1 + \sigma_2$, and $\epsilon = \epsilon_1 = \epsilon_2$.

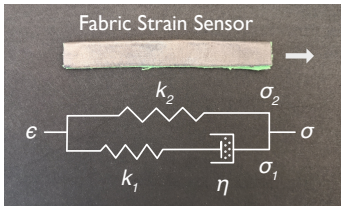

Fig. 11. Approximating a strain fabric using a spring-dashpot model.

According to the basic rule of spring and dashpot ($\sigma_2 = k_2\epsilon_2$ and $\sigma_1 = \eta \cdot \mathrm{d}\epsilon_1/\mathrm{d}t$), we can derive the constitutive equation of this system as

$$\frac{\mathrm{d}\sigma}{\mathrm{d}t} = \frac{\mathrm{d}\sigma_1}{\mathrm{d}t} + \frac{\mathrm{d}\sigma_2}{\mathrm{d}t} = \frac{\mathrm{d}\sigma_1}{\mathrm{d}t} + k_2\frac{\mathrm{d}\epsilon_1}{\mathrm{d}t} = \frac{\mathrm{d}\sigma_1}{\mathrm{d}t} + \frac{1}{\tau}\sigma_1\,, \tag{2}$$

where $\tau = \eta/k_2$ is called the relaxation time constant.

In the stress relaxation state, the deformation value does not change, so $\mathrm{d}\epsilon/\mathrm{d}t = 0$. Since $\sigma = k\epsilon$, we have $\mathrm{d}\sigma/\mathrm{d}t = k \cdot \mathrm{d}\epsilon/\mathrm{d}t = 0$. By setting Eq. (2) to 0, we derive $\mathrm{d}\sigma/\mathrm{d}t = -\sigma/\tau$, assuming $\sigma_1 = \sigma_2 = \sigma/2$ to obtain a closed-form solution. Such constitutive equation links deformation to the stress on the material. By separating variables and integrating

$$\int_{\sigma_0}^{\sigma}\frac{\mathrm{d}\sigma}{\sigma} = -\frac{1}{\tau}\int_0^t \mathrm{d}t\,, \tag{3}$$

we obtain $\sigma(t) = \sigma_0 e^{-\frac{t}{\tau}} + \alpha$, where σ_0 is the initial stress and α is a constant.

Then the relaxation modulus $E_{rel}(t)$ can be derived as

$$E_{rel}(t) = \frac{\sigma\,(t)}{\epsilon_0} = m_1 e^{-\frac{t}{\tau}} + m_2\,, \tag{4}$$

where ϵ_0 is the initial deformation. We fit the relaxation model with experimental data to calibrate parameters m_1, m_2 and τ[1].

4.4 Inference of Joint Angle

With the derived stretch length, the last design element is to infer the joint angle. We analyze the anatomy of human joints to identify the relationship between the deformation and the rotation of joint bones. We then discuss the use of dual strain fabric sensors to enhance sensing robustness.

Human joints can be categorized into six types: synovial joint, pivot joint, hinge joint, saddle joint, condyloid joint and ball and socket joint. Elbow joint is categorized as hinge joint, where the bones can only move along one axis to flex or extend [69]. Similarly to [40], we define the elbow joint angle as the angle between the current position of lower arm and the neutral anatomical position of it. Its moving range is roughly from -10° to 150° [40], and prior works from anatomy have confirmed the relationship between the skin surface deformation and elbow flexion angle [21, 38, 53]. Specifically, three bones are involved in the rotation at the elbow joint: humerus on the upper arm, radius and ulna on the lower arm. As shown in Figure 12, the distal end of the humerus and the proximal heads of the radius and ulna form a small flat triangle-like surface, that is also supported by the collateral ligaments around the elbow. When we wave our arm, the ulna, with its upper

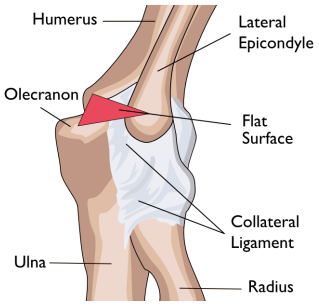

Fig. 12. Anatomy of the elbow joint.

[1]The three parameters of our relaxation model are: m_1 = 0.0233, m_2 = -0.04591, τ = 0.0289. SSE: 0.0795, RMSE: 0.01154.

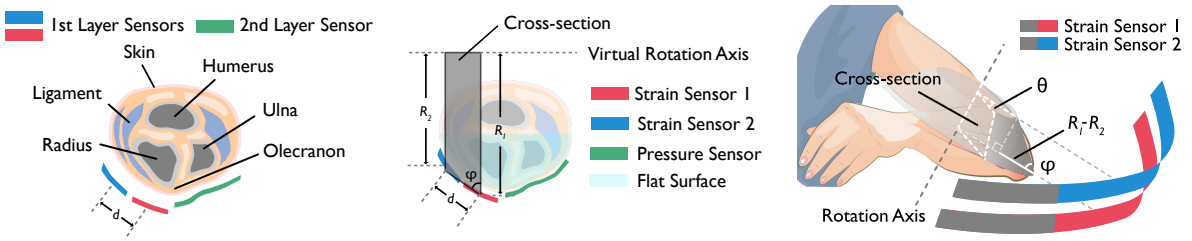

(a) Two layers of sensing fabrics on the elbow: pressure sensor and strain sensors

(b) A trapezoid cross-section (grey) formed around the virtual rotation axis

(c) A circular truncated cone formed by the rotation of cross-section

Fig. 13. Inferring the rotational angle based on the stretch lengths sensed by two strain fabrics. (a) Pressure fabric on the first layer while two strain fabrics on the second layers. (b) We denote the orthogonal distances between strain sensors and virtual rotation axis as R_1 and R_2. The two radiuses, the virtual axis and skin surface slope will form a trapezoid cross-section. The flat surface is also plotted for reference. (c) The rotation of the cross-section will form a circular truncated cone whose top surface radius is the deformation of strain fabric 2 and base radius is that of strain fabric 1. Its height can be computed with distance d and angle φ.

end (called olecranon) will rotate around a virtual rotation axis, and as a result, the triangle-like surface will also rotate in a certain range. The rotation of this flat surface causes the deformation of skin around the joint.

Prior studies have proposed models to describe the relationship between skin deformation and joint rotation [59, 65, 76, 77, 79]. The common problem of all these models is that they assume the virtual rotation axis of the ulna's rotation is known or easy to measure. However, in practice, it is hard to locate this axis because the axis is above the skin with an unknown height. Another problem of these models is that they assume the bulge (i.e., olecranon) of the joint is a perfect horizontal surface, while in fact it tilts with a slope that depends on the shape of the joint bones [16, 26, 92]. To solve these problems, we apply a general model based on anatomy that can cover different joint sizes. We propose two parallel pieces of strain fabric to remove the need of locating the rotation axis.

Sensor Layout. Figure 13(a) and 13(b) show the placement of two strain fabrics together with the pressure fabric. We adopt a two-layer structure to embed the two types of sensing fabrics: the first layer, which is closer to the skin, contains the pressure fabric that is responsible for determining the motion state, while the second layer, which is the outer layer, contains the two strain fabrics. Figure 13 (b) shows the cross-section (grey trapezoid) that rotates with elbow movement. We mark the virtual rotation axis with a dotted line, whose location is unknown to our system. Based on the rotation axis, we draw two parallel radiuses with two strain fabrics as the distal ends. We denote the two radiuses as R_1 and R_2, and the distance between them is d. We denote the inclination angle of flat triangle surface (marked in Figure 12) as φ. R_1 and R_2 are unknown, while d and φ are body parameters that we can measure during calibration.

Dual Input Sensing. Figure 13(c) illustrates how we infer the movement angle with all the parameters we set in the previous step. The extension on the two parallel strain sensors can be seen as two arcs of one virtual circle (whose center is the virtual axis). We denote the length change of each arc as L_1 and L_2 (i.e., stretch lengths of the two strain fabrics) and the rotational angle (supplementary angle of joint angle) as θ. Note that if we view from the projection direction (as shown in Figure 13(c)), the rotation of the cross-section will become a circular truncated cone. With all these parameters, the rotational angle θ can be computed as:

$$\theta = \frac{L_1 - L_2}{R_1 - R_2} = \frac{L_1 - L_2}{d\cos(\varphi)}, \tag{5}$$

where d and φ are calibrated parameters, L_1 and L_2 are the stretch lengths sensed by the two strain fabrics. Thus, we avoid the potential error imported from inaccurate estimation of rotation axis and the radiuses (R_1, R_2).

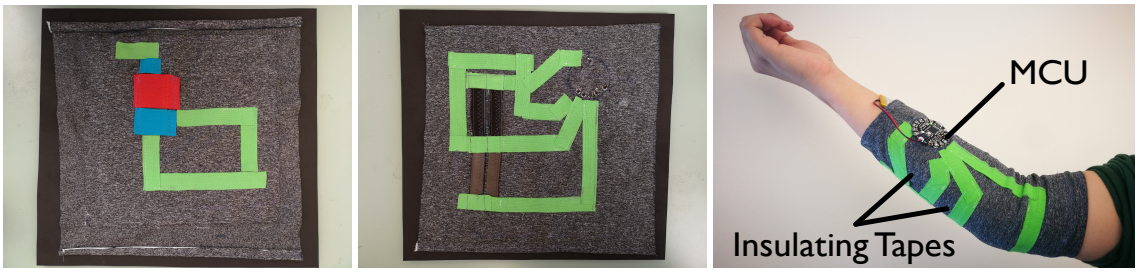

(a) Layer 1 (inner layer) (b) Layer 2 (external layer) (c) Final look

Fig. 14. Integrating strain and pressure sensing fabrics into regular elastic fabrics.

Furthermore, the use of two pieces of strain fabric also allows the system to be robust against small position offsets of these strain fabrics during joint motion. Since the derivation of rotational angle in Eq. (5) uses the difference of two stretch lengths, small position offset of the strain fabrics is canceled out, given that the two strain fabrics are collocated on roughly the same slope of the skin.

We calibrate parameters d and φ based on a user's bone shape and tissue distribution. First, depending on user's joint size and thickness, the distance d between the two strain fabrics can be slightly extended as a user puts on the prototype around a joint. The actual value of d can be measured during a user's first wear of the prototype. Second, φ, the slope of the flat surface around a joint, can differ across users. Since it is not easy to directly measure it on the skin surface, we calibrate it by asking the user to perform a full flexion of a joint, i.e., transitioning from full extension to full flexion. Given the maximal rotational angle $\theta^\star$ of a joint (e.g., the maximal rotation of an elbow joint is around 150° [21, 61, 77]), the angle φ can be computed as $\varphi = \arccos((L_1' - L_2')/d\theta^\star)$ based on Eq. (5), where L_1', L_2' are the stretch lengths of the two strain fabrics during the full flexion. For both parameters (d and φ), their values stay relatively constant for a given user. Thus, the system requires only an one-time calibration for a user, instead of a calibration for every wearing instance even with the same user, entailing a lower calibration overhead than prior works [44, 45, 60, 65].

5 PROTOTYPE IMPLEMENTATION

We build prototypes in two sizes: (1) 27 cm and 31 cm as the lower-elbow and upper-elbow diameter respectively, and (2) 20.5 cm and 23 cm as the lower-elbow and upper-elbow diameter respectively. Each prototype consists of stretchable conductive fabric as strain sensors, inelastic fabric as reference resistor, pressure-sensitive conductive sheet as pressure sensor, stainless steel conductive thread as wires, micro-flex compression knit fabric as layers, sewable snaps and iron-on adhesive hem to connect, sports kinesiology tape to insulate, and a micro-controller (Adafruit Flora). Instead of inventing new high-cost materials, all the components in the system are easy to obtain and at low prices (<$20 except the micro-controller). While aiming to optimize the performance, we also guarantee that the device is comfortable to wear and washable.

5.1 Sensing Fabrics

Layers. We cut two pieces of non-conductive micro-flex knit fabrics [36] as the bases of two layers. As shown in Figure 14(a), in layer 1, the pressure fabric is placed in the inner layer close to the skin so that its resilience can be supported by the outer layer, while in layer 2, the strain fabrics are placed in the outer layer for the maximal degree of extension as in Figure 14(b). This two-layer design structure has two advantages: 1) It provides physical isolation between pressure sensor and strain sensors, so that the deformation on the fabric strain sensors will not be limited by the inelastic pressure sensor. 2) Borrowing idea from PCB manufacture, such double-layer

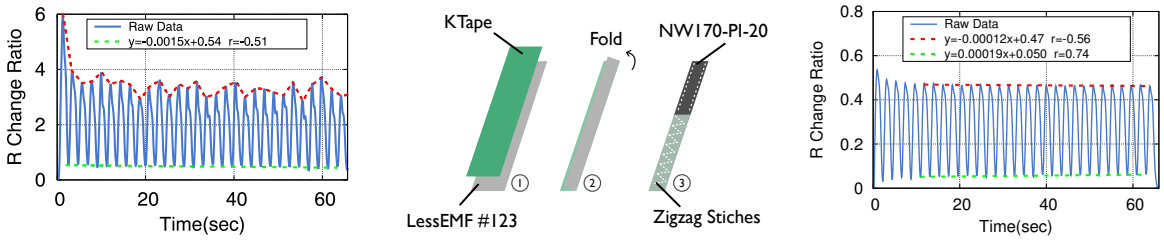

(a) One-layer structure (b) Fabricating two-layer strain fabric (c) Two-layer structure

Fig. 15. One-layer strain fabric leads to mechanical instability over repeated runs (a), while a two-layer structure (b) provides much more stable output (c).

structure can spare more room for the conductive thread to connect different parts because the thread has access to two surfaces now with the help of some connecting holes. For the first advantage, our early-stage prototypes confirmed that, if we put the sensors in the same layer, the closest strain sensors to the pressure sensor can hardly respond to strain because of the shared gap with pressure sensor, though the gap itself is flexible. For advantage two, such design makes the implementation of prototype much easier and also it reveals stronger anti-interference ability than one-layer version, since there is no cross or squeeze of conductive thread on the surface even if we do the vigorous movement. The sensing fabrics on two layers are totally independent and well-insulated from each other. The only connection between the two layers are three conductive sewable snaps so that the circuit on Layer 1 also gets the power supply and transmits voltage value to the micro-controller.

Strain Fabrics. We use LessEMF #A321 [34] as the stretchable conductive fabric, which is silver plated with 76% Nylon and 24% elastic fiber fabric. Our experiments show that a single-layer strain fabric does not offer mechanical stability after repeated stretches, leading to large fluctuating peaks of resistance change ratios over time (Figure 15(a)). To address this issue, we design a two-layer structure, where we paste a layer of insulative elastic tape (KTape [11]) atop the LessEMF fabric, fold it with KTape in the middle and LessEMF on the top and bottom, and then sew these layers with elastic zigzag stitches. The strain sensing fabric is cascaded with an inelastic conductive fabric (EeonTex NM170-PI-20 [70]) serving as the reference resistance. The reference fabric has a similar two-layer structure and layers are sewed using simple inelastic stitches(Figure 16(a) and 16(b)). We do not choose an electrical resistor (e.g., mm-scale SMD resistor) as the reference resistance mainly because connecting a small SMD resistor to the sensing fabric requires soldering the PIN of the resistor to conductive threads. Our experiments show that such soldering introduces much higher noise than that of connecting fabrics via conductive threads. However, we do not rule out SMD resistors as an option and are interested in exploring it in the future.

Figure 15(b) illustrates the fabrication process. Such a two-layer structure improves the stability of output voltage (Figure 15(c)). Specifically, strain fabrics (LessEMF) are cut into pieces of 15 cm × 3 cm in size, resulting in a 1.5cm width sensing fabric after the folding. It is then connected to a 7 cm × 1.5 cm static conductive fabric (EeonTex NM170-PI-20) as the reference resistance. We sew two strain sensors onto Layer 1 using zigzag stitches, which do not influence the elasticity of sensors. They are the main sensing fabrics in our prototype and are placed roughly in accordance with the flat surface of the elbow.

Pressure Fabrics. As we mentioned before, we use 2-layer velostat sandwich structure for our fabric pressure sensor(Figure 16(c)). We place a 3 cm × 4 cm piece of static conductive fabric at the bottom, another 3 cm × 7 cm one on the top and two 3cm×4cm pieces of 1mm-thick pressure-sensitive conductive sheet [72] in between(Figure 16(d)). Both the top and bottom layers perform as reference resistors and have an extra part as pins to connect with conductive threads. We use iron-on adhesive hem to stick them together and cover the sensor with kinesiology tape to fasten and insulate. As pressure that elbow exerts on the sensor without

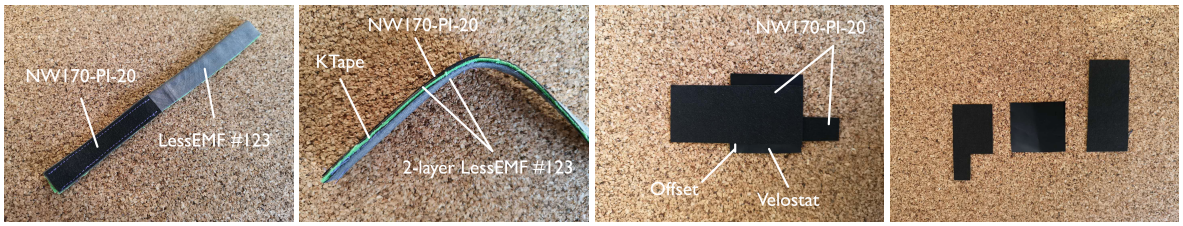

(a) Two-layer strain fabric (b) Two-layer strain fabric (side) (c) Two-layer pressure fabric (d) Pressure fabric components

Fig. 16. Strain and pressure fabrics.

any supporter contributes more to spatial deformation rather than forming a sagging area , we sew a piece of stretched highly-elastic fabric [35] outside the sensor unit to provide a reversed pressure while bending arms. The pressure sensor is laid on Layer 2 beside two strain sensors on Layer 1 and exactly covers the olecranon part of elbow (Section 4.4). The final look of our prototype is shown in Figure 14(c).

5.2 Computing Unit

We use an Adafruit FLORA v2 board whose core board is ATmega 32u4 to digitize analog voltage signals of each sensor. FLORA is a small (1.75" diameter, weighing 4.4 grams) and fabric friendly board with sewing tap pads, which interferes little with motions and can be sewed on the sleeves. ATmega 32u4 is an 8-bit micro-controller with 32K bytes of ISP Flash. During signal digitization, we use 250kHz ADC rate, which is sufficient in capturing low-frequency motions. Timer frequency is 100Hz and results are stored in the MCU. We sew eight conductive snaps on the layers, among which three electrically connect two layers and five attach the sewing tap pads on Flora to Layer 1 so that the micro-controller is detachable. Also, We sew conductive threads into the layers as leads to connect three sensors with the micro-controller.

5.3 Points for Attention in Fabrication Process

We summarize a few points for attention on the prototype fabrication. First, when we use conductive threads as the leads to connect the pressure sensor with the snaps, the intersection between the threads and the sensor requires a piece of conductive elastic fabric. This is because the pressure fabric is inelastic, which will leave more gaps between the threads and the fabric, causing sharp increases in resistance. Since we rely on resistance change ratio to determine the loading or unloading state, a large resistance value will lead to low sensitivity to small resistance change. Another suggestion for sewing is to place the conductive thread in the bottom bobbin, given that the conductive thread is too thick to go through the hole of the sewing machine. Finally, with the two-layer design, the outer layer can also possibly contact human skin, which would introduce signal interference. To physically isolate layers and shield against unwanted touch, we cover all the conductive threads with KTape.

Although our current fabrication process is lengthy with manual efforts, most of the time-consuming steps (e.g., cutting, sewing, folding) can potentially be automated in the future to scale up the fabrication process. The exact placement of various sensing fabrics during the assembling is based on the typical size of the bulge of human elbow joint, and thus can be realized as a repeatable process. We will discuss more on the automation of fabrication process in Section 8.

6 EVALUATION

We have recruited 10 participants from our local institution to evaluate our prototype. The detailed user information is summarized in Table 2 and Table 3. In this section, we will first describe the experiment setup and the method of collecting the ground truth. Then the system accuracy is demonstrated given various movement

Table 2. Information of ten participants in the evaluation.

	Gender		Height/cm			Weight/kg		
	Male	Female	<170	170 - 180	>180	<60	60 - 80	>80
# of Users	7	3	2	4	4	3	4	3

Table 3. The upper and lower arm size of each participant.

User ID	1	2	3	4	5	6	7	8	9	10
Upper Arm Size (cm)	31	29.5	30	32	27.5	23	24.5	22.5	23	23
Lower Arm Size (cm)	27	22.5	23.5	24	24.5	21.5	25	23	20.5	22

patterns. We further examine the reliability of our system regarding the sensor movement and washability. Finally, we will examine the comfort level of the prototype via a user study.

Setup. Each participant is instructed to wear the prototype with the size that fits his/her arm. With two available sizes of the prototype (Section 5), participants whose upper arms are with perimeters larger than 24 cm wear the larger size. Various types of motion patterns are designed and demonstrated in videos. After watching the video, participants imitate the motion, while the prototype records fabric sensing data, which are then transmitted to a laptop running the joint angle inference algorithm. In the end of the experiment, each participant fills in a questionnaire to rate the level of tightness, comfort and flexibility of wearing the fabric prototype, as well as their feedback on the one-time calibration. Additional feedback is also solicited on the comparison of our prototype and commercial compression sleeves.

To collect ground truth data, we choose the Vicon system [9] because of its higher accuracy in comparison to other motion-capture systems such as Kinect. Its sensing ability relies on the reflective skin markers and infrared cameras and the system error is less than 2 mm [51]. We attach optical markers to each participant's elbow to measure the skin deformation and elbow angle. Our early tests reveal that with only three markers attached to the arm (on upper arm, elbow joint and lower arm respectively), Vicon occasionally loses track of the markers as these small markers can be easily occluded. To address this problem, we create two rigid planes with hard paper board and place them onto the upper and lower arm skin surface. These planes reduce occlusions and help Vicon track the arms and output the joint angle even if one or two points on the plane are missing. Meanwhile, to synchronize and compare data from Vicon and our system in real time, we develop a cross-platform tool programmed in C to gather data from MCU and Vicon system together. We integrate the calibration procedure into the tool. The experiment with each participant takes roughly 40 minutes, where calibration and adjustment takes only three minutes.

6.1 Accuracy of Inferring Joint Angles

We start by examining the accuracy of sensing joint angles using our fabric prototypes. Specifically, the following sequence of motions is designed for each participant:

(1) Flex the elbow by various degrees (i.e., 45°, 90°, and 150°), and repeat the motion at three levels of speed. Repeat each motion three times and then rest 30 seconds in the end.
(2) Repeat the above motion sequence at the same three levels of speed but pause 5 seconds at 45°, 90°, and 150°. Rest 30 seconds after this step.
(3) Perform free-form motions, including waving tennis racket, performing the yoga tree pose and belly button challenge.

The first two steps are controlled motions for evaluating the efficacy of various design elements to handle different movement angles and speed. Specifically, by adding the 5-second pause, step (2) is meant to examine the efficacy of the design element on stress relaxation and drift compensation (Section 4.3). The third step evaluates the system under free-form motions.

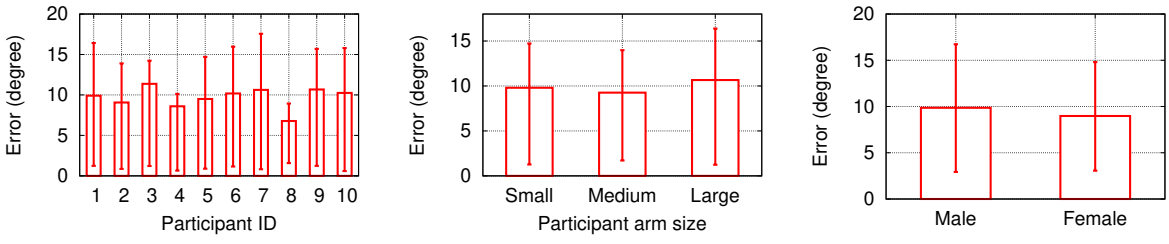

Fig. 17. Overall accuracy in inferring joint angles, including the average accuracy of each participant (a), the impact of arm size on angular errors (b), and the overall accuracy for each gender (c).

We next discuss our results, starting from overall accuracy and then diving into the analysis on controlled and free-form motions. We evaluate accuracy by calculating absolute joint angular errors, i.e., the absolute differences between inferred and ground-truth joint angles.

6.1.1 Overall Accuracy. We evaluate system's overall accuracy by aggregating joint angular errors of all participants in performing all steps of the motion sequence. Figure 17(a) plots the average angular error for each participant, where error bars represent the range between the 5-th and 95-th percentiles. Overall, the median accuracy across users is 9.69°, which can facilitate rehabilitation applications [85] that aim to limit the range for patient's joint movement (e.g., from 30°-100°). Comparing results across participants, we observe that the average angular error with participant 8 is the lowest. This is because the arm size of this participant is used as the reference for building the fabric prototype worn by this participant. The prototype best fits this participant.

We further analyze the impact of participant's arm size on joint angular error. We divide participants into three groups based on the perimeters of their upper arms: small (upper arm perimeter < 24 cm), medium (24 cm ≤ upper arm perimeter ≤ 28 cm), and large (upper arm perimeter > 28 cm). We focus on the size of the upper arm because lower arm size has almost no impact on wearing tightness. We aggregate joint angular errors of participants in each group, and plot the average as well as the 5-th and 95-th percentiles for each group in Figure 17(b). We observe that for participants with medium arm size, their average joint angular error is the lowest. This is because the prototypes best fit these participants without being too loose or tight. Too tight contact between skin and fabric sensor limits the spatial deformation of velostat material, which causes errors in motion state determination. On the other hand, when the prototype is too loose, the fabric fails to capture minor skin deformation, which also leads to larger errors.

We also examine the overall accuracy for male and female participants. Figure 17(c) plots the average with error bars covering the 5-th and 95-th percentiles. We do not observe differences with statistical significance. This is expected as their arms have the same anatomic structure.

6.1.2 Controlled Motion. We now zoom in on results of controlled motions (step (1) and (2)), aiming to examine the impact of pause, motion speed, and flexion angle on the accuracy of sensing joint angles.

Pause. To analyze the impact of pause at different stress levels, we aggregate the angular errors in step (1), where there is no pause between joint movement. We compare them to that in step (2), where 5-second pause is added. Figure 18(a) compares the CDFs. We observe negligible differences between the distributions. It indicates that the system can track continuous joint motion while controlling the error accumulation, thanks to the design element on stress relaxation and drift compensation (Section 4.3) that deals with the drift error. However, the distribution of errors during continuous motion has a slightly longer tail, with the maximal error of 38.7°, compared to the maximal error of 34.3° during motions with 5-second pause. We hypothesize that the longer tail is due to the

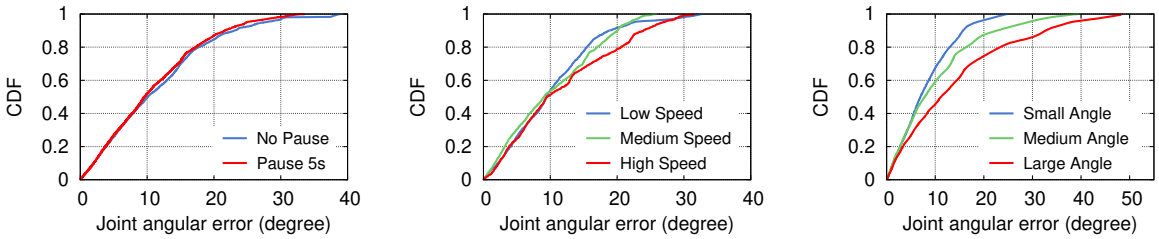

Fig. 18. Accuracy of inferring joint angles under controlled motions, where we vary the pause between adjacent movement (a), movement speed (b), and flexion angles (c).

extra arm vibration that seemingly occurs during continuous motions. In the experiments, we observe when participants continuously flex their elbows, their arms slightly shake in the end of each flexion. The shaking results in vibration of fabric strain sensors and occasion peaks in angular errors.

Speed. Speed is another factor that may affect sensing accuracy. We evaluate our prototype with three levels of speed: low speed (20°/s), medium speed (50°/s), and high speed (80°/s). As shown in Figure 18(b), higher speed causes larger errors, while for the low speed, 80% of errors are within 15°. Given that the modulus we use for stress relaxation and drift is time-dependent, it is likely that the relaxation is loosely related to speed. Another possible reason is that for higher speed, the fixed window size (12) used by the motion detection algorithm (Algorithm 1) may be not wide enough for the regression kernel to reconstruct the curve. The confused motion detector may output some unreliable motion status at high speed. In future work, we plan to develop a window-size selection module that adapts the window size to the current speed. It is challenging since practical movement is not controlled and speed can vary every moment. We will seek methods to estimate speed in real time so that the window size can be adapted properly.

Flexion Angle. We also examine whether the actual flexion angle affects the resulting joint angular error. We divide angular errors into three groups based on the actual flexion angle: small (0-45°), medium (45°-90°) and large (90°-150°). Figure 18(c) compares the accuracy results for motions with different flexion angles. We observe that larger flexion angles lead to slightly larger angular errors. Specifically, the median error under small flexion angles is 9.71° with 31.03° as the 95-th percentile, which increases to 13.24° with 37.21° at its 95-th percentile under large flexion angles. We hypothesize that this trend is due to the influence of deformation in wale direction. When the flexion angle exceeds 90°, the contact of the upper and lower arm forces the strain sensor to extend in the wale direction. Given that resistance change along fabric's wale direction is less sensitive to the extension (Section 2), it is difficult to capture small extensions, resulting into larger errors. To mitigate this problem, we will explore other methods to capture extension in the wale direction in future work.

6.1.3 Free-Form Motion. We further examine sensing accuracy under free-form motions. Specifically, we consider the following motions: 1) waving a tennis racket several times, to check the performance of our system at high speed and in wide range of elbow flexion; 2) tree pose from yoga, to examine the ability of reconstructing motionless and steady gesture; 3) belly button challenge, a popular movement among young people to test body flexibility, which requires using one hand to touch one's belly button from the other side across the back. We expect to see similar performance when the elbow movement is done with some full-body motion.

Figure 19 plots joint angular errors for the above three motions. We obtain three key observations. First, slow movements (e.g., tree pose, belly button) in general achieve higher accuracy with our prototype. This is because of the slow restoration procedure of the fabric under sudden strain, which introduces larger errors when tracking quick motions. Second, belly button motion leads to higher errors than the tree pose. We hypothesize that it is

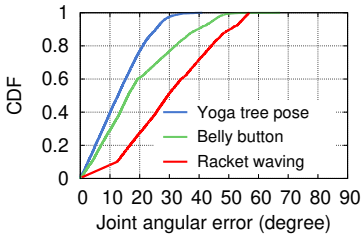

Fig. 19. Accuracy of inferring joint angles under three free-form motions.

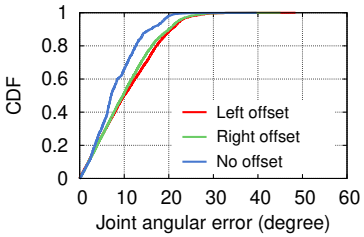

Fig. 20. Impact of fabric displacement on sensing accuracy.

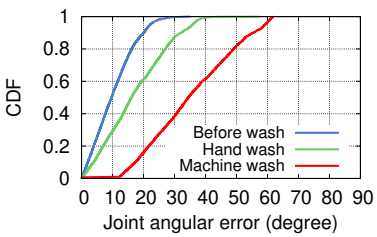

Fig. 21. Impact of wash on fabric's sensing performance.

due to the rotation of lower arm and wrist during this motion. Since the prototype is currently designed to track mainly elbow flexion, joint rotation in other degrees of freedom introduces extra deformation and pressure and can interfere with the sensing of joint angle. Finally, similarly to our prior results on speed and flexion angle, motions (racket waving) with larger flexion angles and higher speeds lead to higher errors. During these motions, we observe more wrinkles accumulated around the fabric of the elbow region. Wrinkles affect fabric resistance and cause larger errors in inferring joint angles. In Section 8, we will discuss our future work to better deal with wrinkles.

6.2 Sensing Robustness

After examining the sensing accuracy, we now move on to evaluating the sensing robustness of our fabric prototypes. We focus on two practical factors that can affect fabric's sensing performance: 1) the displacement of sensing fabric around the joint region, which can be caused either by initial wearing or by later motions; and 2) repeated wash of the fabric prototype after the MCU is detached.

Fabric Displacement. The prototype performs the best when the sensing fabrics are placed in the right region of the elbow: the two strain fabrics are right around the ulna bone while the pressure fabric is right around the radius bone (Figure 13). In practice, however, these sensing fabrics can slightly shift away from their best sensing spots, either because of continuous joint motion or the improper alignment during the initial wearing. To evaluate the impact of fabric displacement, we instruct one participant to wear the prototype and flex the elbow by various angles (45°, 90°, and 150°) with a speed of 20°/s. We emulate fabric displacement by slightly moving the sensing fabrics from their optimal sensing spots by 1 cm, either to the left or to the right. We then compare the results to that without any offset to examine the impact of fabric displacement on sensing accuracy.

Figure 20 plots the CDFs of angular errors with and without fabric displacement. As expected, offsets from the center/optimal position slightly increase the joint angular error. The main reason is that these small offsets cause one of the strain fabrics to move beyond the olecranon, which breaks the parallelism of the two fabrics. This introduces error in calculating the angle from the differential inputs. Displacement with the right-side offset leads to slightly smaller errors because the pressure fabric is on the left of the strain fabrics. As a result, moving to the right has less influence on the pressure fabric. Note that in practice, larger displacement can be easily noticed and corrected by simply placing the fabrics to the center of the elbow. Overall, the results reveal that small offsets ($\leq$1 cm) introduce a minor increase in joint angular errors, demonstrating the efficacy of the dual input sensing (Section 4.4) in dealing with motion artifact.

Washability. Washability is essential to long-term uses of the fabric prototype. The only electrical component of our prototype is MCU, which can be easily detached through a button (Section 5.2), leaving the rest of the prototype washable. To examine the impact of wash on the fabric's sensing ability, we test two types of washing:

machine wash and hand hash, where the latter is more gentle. We instruct a participant to wear the prototype before and after washing to perform all steps of motion sequence and compare the errors in inferring joint angles.

Figure 21 compares the CDFs of joint angular errors before and after wash. We observe that both types of wash degrade fabric's sensing performance. This is partially because fabrics shrink to some extent after wash, even if we dry the prototype thoroughly in open air. In comparison, machine wash affects the performance more severely, resulting into a median angular error of 34.1° and a maximum error of 72.4°. This is mainly because after machine wash, some conductive threads are broken while others have loose contact with the fabric. Both greatly affect the sensing of resistance change ratios. Gentle hand wash, on the other hand, can better protect the conductive threads and cause minor degradation (7.64°) to the sensing performance. In future work, we are interested in further improving the prototype's robustness against wash through better fabrication. We will also conduct longer-term studies to examine the impact of repeated washes (Section 8).

6.3 Comfort Level

To evaluate the comfort level of our prototypes, we conduct a user study with ten participants to solicit their input. All participants of our experiments are asked to fill in a questionnaire. The questionnaire asks participants to rate with the scale of 1–9 the following attributes of the prototype system: (1) tightness (1-too tight, painful to wear; 9-very loose, do not feel wearing it at all), (2) flexibility (1-too rigid, cannot perform any motion; 9-very flexible, no hindrance to performing any activities), (3) one-time calibration in the beginning (1-too long, tedious; 9-quick, not an overhead at all), and (4) the overall comfort level of wearing our prototype (1-very uncomfortable; 9-very comfortable, do not mind wearing it at all times).

We calculate the average ratings of the above four attributes, and they are 6.1, 8.5, 8.3 and 8.8 respectively. It demonstrates that our prototype achieves an acceptable comfort level: the sizes of our prototype well adapt to target users with different figures; the prototype does not hinder motions for sports and everyday use; one-time calibration after purchasing it is relatively quick and acceptable. Additionally, 9 participants think applying our system into the teaching process of certain sports like yoga or gymnastics would be very helpful (8 points or more) to their progress. All the participants are willing to purchase such a system for $30-$40.

Additionally, we have also solicited participant feedback comparing the comfort level of our prototype with other commercial sleeves. We invite participants to wear off-the-shelf compression sleeves [1, 2] for 30 minutes, which roughly the same duration of wearing our fabric prototype during the experiment. Overall, participants have not mentioned any issues related to wear comfort using our prototype. A participant (P5) comments that "There is no difference between wearing your prototype and the compression sleeves.". Another participant (P2) comments that " When you are playing sports, this would not have any influence just as the protection arm sleeves, while it tightness might make you feel a little bit uncomfortable when you are typing before a computer.".

7 RELATED WORK

We divide existing works on fabric sensing into two main categories based on their sensing capabilities.

Motion Classification. The first category of works focus on differentiating a pre-defined set of motions or activities. In particular, two types of resistive fabric strain sensors have been explored in the past.

The first type is made of textile structure with conductive yarns. The embedded conductive yarns form many conductive paths, where contact resistance would change following the given mechanical stretch. Atalay et al. [12] chose to use silver yarn and nylon as the material and produced a weft-knitted strain sensor. Zhang et al. [89] created knitted strain sensors by using stainless steel and carbon yearns. The advantage of this kind of strain sensor is that the integration of the conductive medium into the textile structure is easily accomplished by slightly modifying existing knitting machine procedure. However, the mixture or the filling material of the sensing yarn is always rigid, which may cause discomfort while wearing it.

The other type is to coat elastic material (e.g., lycra) by intrinsically conductive polymer (ICP). In 1997, Lorussi et al. [46] developed a PPy-coated Lycra fabric and presented a wearable system able to reveal the status of body kinematic chains. Oh et al. [57] coated PPy on Nylon-spandex(95:5) and obtained a strain sensor which can keep sensing until 60% extension. Irmandy et al. [82] used off-the-shelf PPy-coated fabric LTT-SLPA(28% Elastane, 72% Nylon) made by EEONYX Inc. to develop a deformable musical keyboard. They suggested that the maximum strain the sensor could handle is around 100-150%, which indicates this fabric is ideal for wearable strain sensor as its working space is large enough for skin surface deformation happening on our body.

We are inspired by these prior works on fabric sensing. Our work differs in that our system achieves much higher sensing granularity by enabling the inference of actual joint angles, rather than differentiating pre-defined gestures or poses.

Motion Reconstruction. The second category of works aim to compute joint angles. Most of these works rely on specially-designed materials. As examples, Mattmann et al. [49] used a novel thermoplastic elastomer strain sensor and attached it to the back of a tight-fitting cloth to recognize upper body postures. Menguc et al. [50] pour liquid silicone on a 3D print mold and inject EGaIn to generate a soft strain sensor. Bae et al. [13] chose graphene, a special carbon structure as its base, made a transparent strain sensor detecting the motion of a finger. Ali et al. [37] designed functionalized fabric to measure triboelectric charges induced by fabric deformation, making it possible to differentiate joint movement types (extension, flexion) and movement speed with the loose-fitting cloth. All these strain sensors require complicated chemical procedure and special techniques, which entail a higher manufacturing cost. Our work differs in that we examine the use of off-the-shelf, low-cost fabrics for fine-grained joint motion sensing.

Additionally, fiber has also been explored for joint motion sensing. Peter et al. [27] incorporated conductive fibers into the fabric with elastic cord and sensed the joint angle according to the resistance change of conductive fibers. Massimiliano et al. [24] made use of optical fiber, which measures the relative angle in a rotating joint based on the intensity modulation of a laser beam propagating in a single-mode optical fiber. Sunghoon et al. [43] developed a sensing system comprising a retractable reel, a string and a potentiometer. This system estimates the joint angle accurately under fast movement settings with the help of the retractable reel. Our work differs in that we study a different approach using off-the-shelf, low-cost fabrics, which potentially can be more flexible, and more comfortable to wear compared to fibers and reels.

Other motion-reconstruction systems involving fabric sensing combine fabric sensors with other types of sensors. Examples include E-Skin by Xenon [10], on-body sensing system by FIGUR8 [5] and super soft stretch sensor by stretch sense [7]. Besides sensing fabric, E-Skin system places 3-axis accelerometers and 3-axis gyro sensors on the plastic part on the chest [3]. Stretch sensor attaches an extra circuit unit at the end of its smart garments [8]. Adrian [23] used the wearable inertial measurement units (IMUs) to estimate the "movement skill". FIGUR8 claims to use 9-axis inertial measuring unit [4] in its products. Our work differs in that we reconstruct joint motion solely based on fabric sensing without the aid from other types of sensors.

8 CONCLUSION AND FUTURE WORK

In this work, we studied the use of off-the-shelf conductive fabrics to sense the strain and pressure during joint motion and infer joint rotational angle. To achieve accurate and robust sensing, challenges arising from the inherent properties of fabric materials are addressed. Our work leveraged models from material science and biomechanics to characterize fabric properties and the relationship between skin deformation and joint angle. We fabricated prototypes with off-the-shelf fabrics and a micro-controller. The system's sensing accuracy, robustness, and comfort are demonstrated by conducting system experiments and user studies with 10 participants.

We recognize the limitations of our current study and summarize our ongoing and future work as follows:

- We currently fabricated prototypes only for the elbow joint. Moving forward, we plan to fabricate prototypes for other types of body joints and examine the efficacy of our design. The general design principle still applies and we will need to consider the anatomy of other joint types for possible adjustments on inferring joint angle. For joints such as wrists with larger degrees of freedom during rotation and capable of performing more types of rotational movement, we will consider optimizing the current design and arrangement of sensing fabrics to maximize the number of rotation types the system is capable of tracking.
- Since our sensing fabrics are conductive, sweat can affect their conductivity and interfere with fabric sensing. We have not noticed any participant sweating during the experiment, thus the impact of sweat on the sensing performance is still unknown. In the future, we will test our prototypes with users performing vigorous exercises to examine the system performance under excessive sweating. We will explore thinner fabrics to help the body better dissipate heat. Also, we will consider arranging insulative layers close to skin to protect sensing fabrics and the few conductive threads connecting to the micro-controller from sweat.
- From experiments we noticed that when the sensing fabric is not well fitting the joint surface, joint motion occasionally wrinkles the fabric, which affects fabric resistance and causes larger errors in inferring joint angles. This issue is partially due to limited (two) size options of current prototypes, which do not fit well for some participants. We plan to fabricate prototypes in more sizes to ensure exact tightness and reduce wrinkles. We will also consider designing prototypes with adjustable sizes using the nylon fastener tape. Additionally, we will explore fabrics with better elasticity so that they can retract/stretch more quickly to better fit joint surface during fast motion.
- The current fabrication of the fabric prototype involves lengthy human efforts. We are interested in examining possible automation of certain steps to expedite the fabrication process. Most fabrication efforts have been on cutting, folding, and sewing the fabrics, which potentially can be automated by machines for mass production. The assembling of various fabric pieces needs only knowledge on the typical size of the bulge of the joint to ensure that sensing fabrics are properly placed to sense skin deformation and pressure. Since the fabric prototype will be fabricated in a small number of size options, for users fitting in the same size, their individual differences in the size of joint bulge would be small and can be handled by the dual sensing design (Section 4.4) to ensure sensing robustness. Thus, the fabric assembling does not need to be conducted on a per-user basis and can potentially be made repeatable.
- We recognize the limitations of our current user study, which is based on a small user population and short-term wearing experiences. We plan to fabricate more prototypes, expand our user base, and solicit feedback after more diverse activities. We will also conduct longer-term studies to examine the durability of the system (especially after repeated washes) and user experience on fabric's overall comfort, flexibility, tightness after long-time wear. We are reaching out to orthopedists at a local hospital to discuss possible deployment of our prototypes for monitoring joint recovery after surgeries.

ACKNOWLEDGMENTS

We sincerely thank reviewers for their insightful comments and suggestions that helped improve the paper. This work is in part supported by the Neukom CompX Faculty Grant at Dartmouth College, and National Science Foundation under IIS-1822819. Any opinions, findings, and conclusions or recommendations expressed in this material are those of the authors and do not necessarily reflect those of the funding agencies or others.

REFERENCES

[1] 2018. Compression Arm Sleeve. https://www.amazon.com/d/Elbow-Braces/Kunto-Fitness-Compression-Tendonitis-Treatment/B010P9Q13K/ref=sr_1_1_sspa?s=sporting-goods&ie=UTF8&qid=1542318962&sr=1-1-spons&keywords=Compression+Arm+Sleeve&psc=1

[2] 2018. Compression Sleeve. https://www.amazon.com/McDavid-Compression-Protection-Basketball-Baseball/dp/B016WZG6KO?ref_=Oct_BSellerC_9590773011_4&pf_rd_p=329f6528-119f-5272-a932-88cab21c7435&pf_rd_s=merchandised-search-6&pf_rd_t=101&pf_rd_i=9590773011&pf_rd_m=ATVPDKIKX0DER&pf_rd_r=39BDF952GDARHYTKSK6H&pf_rd_r=39BDF952GDARHYTKSK6H&pf_rd_p=329f6528-119f-5272-a932-88cab21c7435

[3] 2018. E-Skin Sensor. https://xenoma.com/eskin-dk

[4] 2018. Figur 8 Sensors. https://figur8tech.com/pages/research-and-development-kit

[5] 2018. Figur8 Tech. https://figur8tech.com/blogs/figur8

[6] 2018. Rehabilitation Gui delines for Elbow Ulnar Collateral Ligament (UCL) Reconstruction. https://www.uwhealth.org/files/uwhealth/docs/sportsmed/SM_UCL_reconstruction.pdf

[7] 2018. Stretch Sense. https://www.stretchsense.com/stretch-sensors/

[8] 2018. Stretch Sense Circuit. https://www.stretchsense.com/smart-garments/

[9] 2018. Vicon. https://www.vicon.com/

[10] 2018. Xenoma E-Skin. https://xenoma.com/

[11] Amazon. 2018. Kinesiology Tape. https://www.amazon.com/KT-Tape-Kinesiology-Therapeutic-Sports/dp/B003DV9JGO/ref=sr_1_1/136-0678870-8281028?s=sports-and-fitness&ie=UTF8&qid=1533589584&sr=1-1&refinements=p_4%3AKT+Tape

[12] Ozgur Atalay, William Richard Kennon, and Erhan Demirok. 2015. Weft-Knitted Strain Sensor for Monitoring Respiratory Rate and Its Electro-Mechanical Modeling. *IEEE Sensors …* 15, 1 (2015), 110–122.

[13] S H Bae, Y Lee, B K Sharma, H J Lee, J H Kim, and J H Ahn. 2013. Graphene-based transparent strain sensor. *Carbon* 51 (2013), 236–242.

[14] Abdelkareem Bedri, Richard Li, Malcolm Haynes, Raj Prateek Kosaraju, Ishaan Grover, Temiloluwa Prioleau, Min Yan Beh, Mayank Goel, Thad Starner, and Gregory Abowd. 2017. EarBit: Using Wearable Sensors to Detect Eating Episodes in Unconstrained Environments. *Proceedings of the ACM on Interactive, Mobile, Wearable and Ubiquitous Technologies* 1, 3 (Sept. 2017), 37–20.

[15] Mary Ellen Berglund, Julia Duvall, and Lucy E Dunne. 2016. A survey of the historical scope and current trends of wearable technology applications. *ISWC* (2016), 40–43.

[16] Ceren Günenç Beşer, Deniz Demiryürek, Hakan Özsoy, Burcu Erçakmak, Mutlu Hayran, Onur Kızılay, and Arzu Özsoy. 2014. Redefining the proximal ulna anatomy. *Surgical and Radiologic Anatomy* 36, 10 (July 2014), 1023–1031.

[17] T Bhattacharjee, A Jain, S Vaish, M D Killpack, and C C Kemp. 2013. Tactile sensing over articulated joints with stretchable sensors. In *2013 World Haptics Conference (WHC 2013)*. IEEE, 103–108.

[18] Johann Borenstein, Lauro Ojeda, and Surat Kwanmuang. 2009. Heuristic reduction of gyro drift in IMU-based personnel tracking systems. In *SPIE Defense, Security, and Sensing*, Craig S Halvorson, Šárka O Southern, B V K Vijaya Kumar, Salil Prabhakar, and Arun A Ross (Eds.). SPIE, 73061H.

[19] Toni E Campbell, Bridget J Munro, Gordon G Wallace, and Julie R Steele. 2007. Can fabric sensors monitor breast motion? *Journal of Biomechanics* 40, 13 (2007), 3056–3059.

[20] Gerard Canal, Sergio Escalera, and Cecilio Angulo. 2016. A real-time Human-Robot Interaction system based on gestures for assistive scenarios. *Computer Vision and Image Understanding* 149 (2016), 65 – 77. https://doi.org/10.1016/j.cviu.2016.03.004

[21] Matthieu K Chardon, Yasin Y Dhaher, Nina I Suresh, Giselle Jaramillo, and W Zev Rymer. 2015. Estimation of musculotendon kinematics under controlled tendon indentation. *Journal of Biomechanics* 48, 13 (Oct. 2015), 3568–3576.

[22] Philo Tan Chua, R. Crivella, B. Daly, Ning Hu, R. Schaaf, D. Ventura, T. Camill, J. Hodgins, and R. Pausch. 2003. Training for physical tasks in virtual environments: Tai Chi. In *IEEE Virtual Reality, 2003. Proceedings.* 87–94. https://doi.org/10.1109/VR.2003.1191125

[23] A. Derungs, S. Soller, A. Weishäupl, J. Bleuel, G. Berschin, and O. Amft. 2018. Regression-based, mistake-driven movement skill estimation in Nordic Walking using wearable inertial sensors. In *2018 IEEE International Conference on Pervasive Computing and Communications (PerCom)*. 1–10. https://doi.org/10.1109/PERCOM.2018.8444576

[24] M. Donno, E. Palange, F. Di Nicola, G. Bucci, and F. Ciancetta. 2008. A New Flexible Optical Fiber Goniometer for Dynamic Angular Measurements: Application to Human Joint Movement Monitoring. *IEEE Transactions on Instrumentation and Measurement* 57, 8 (Aug 2008), 1614–1620. https://doi.org/10.1109/TIM.2008.925336

[25] Tsutomu Fujimura. 2012. Investigation of the relationship between wrinkle formation and deformation of the skin using three-dimensional motion analysis. *Skin Research and Technology* 19, 1 (June 2012), e318–e324.

[26] Shin-ichi Fujiwara, Hajime Taru, and Daisuke Suzuki. 2010. Shape of articular surface of crocodilian (Archosauria) elbow joints and its relevance to sauropsids. *Journal of Morphology* 1 (2010), NA–NA.

[27] Peter T. Gibbs and HHarry Asada. 2005. Wearable Conductive Fiber Sensors for Multi-Axis Human Joint Angle Measurements. *Journal of NeuroEngineering and Rehabilitation* 2, 1 (02 Mar 2005), 7. https://doi.org/10.1186/1743-0003-2-7

[28] Guido Gioberto and Lucy E Dunne. 2012. Garment Positioning and Drift in Garment-Integrated Wearable Sensing. In *2012 16th Annual International Symposium on Wearable Computers (ISWC)*. IEEE, 64–71.

[29] R. Gnanadesikan. 1977. *Methods for statistical data analysis of multivariate observations / R. Gnanadesikan.* Wiley New York. x, 311 p. : pages.

[30] Linsey Griffin, Crystal Compton, and Lucy E Dunne. 2016. An analysis of the variability of anatomical body references within ready-to-wear garment sizes. In *Proceedings of the 2016 ACM International Symposium on Wearable Computers - ISWC '16*.

[31] H Harms, O Amft, and D Roggen. 2009. Rapid prototyping of smart garments for activity-aware applications. *Journal of Ambient ...* (2009).

[32] Ragnar Holm. 1967. Electric Contacts. Springer Berlin Heidelberg, Berlin, Heidelberg.

[33] https://academic.csuohio.edu/. 2018. Linear Viscoelasticity. https://academic.csuohio.edu/duffy_s/Linear_Visco.pdf

[34] LessEMF Inc. 2018. Stretch Conductive Fabric. Retrieved Aug 4, 2018 from https://www.lessemf.com/321.pdf

[35] Joaan. 2018. Superflex Performance Fabric. https://www.joann.com/superflex-compression-performance-fabric-black/15226897.html#q=performance%2Bfabric&prefn1=prod_type&sz=36&start=37&prefv1=Product

[36] Joann.com. 2018. Micro-Flex Knit Fabric. Retrieved Aug 10, 2018 from https://www.joann.com/loungeletics-performance-micro-flex-compression-knit-fabric-59-heather/15781511.html

[37] Ali Kiaghadi, Morgan Baima, Jeremy Gummeson, Trisha Andrew, and Deepak Ganesan. 2018. Fabric as a Sensor: Towards Unobtrusive Sensing of Human Behavior with Triboelectric Textiles. In *Proceedings of the 16th ACM Conference on Embedded Networked Sensor Systems, SenSys 2018, Shenzhen, China, November 4-7, 2018*. 199–210. https://doi.org/10.1145/3274783.3274845

[38] Laurel Kuxhaus, Sisi Zeng, and Charles J Robinson. 2014. Dependence of elbow joint stiffness measurements on speed, angle, and muscle contraction level. *Journal of Biomechanics* 47, 5 (March 2014), 1234–1237.

[39] Yordan Kyosev. 2018. Narrow and Smart Textiles. Springer International Publishing, Cham.

[40] S Laksanacharoen and S Wongsiri. [n. d.]. Design of apparatus to study human elbow joint motion. In *IEEE EMBS Asian-Pacific Conference on Biomedical Engineering, 2003*. IEEE, 236–237.

[41] Alberto Leardini, Lorenzo Chiari, Ugo Della Croce, and Aurelio Cappozzo. 2005. Human movement analysis using stereophotogrammetry. *Gait & Posture* 21, 2 (Feb. 2005), 212–225.

[42] Jaehong Lee, Hyukho Kwon, Jungmok Seo, Sera Shin, Ja Hoon Koo, Changhyun Pang, Seungbae Son, Jae Hyung Kim, Yong Hoon Jang, Dae Eun Kim, and Taeyoon Lee. 2015. Conductive Fiber-Based Ultrasensitive Textile Pressure Sensor for Wearable Electronics. 27, 15 (2015), 2433–2439.

[43] S. I. Lee, J. Daneault, L. Weydert, and P. Bonato. 2016. A novel flexible wearable sensor for estimating joint-angles. In *2016 IEEE 13th International Conference on Wearable and Implantable Body Sensor Networks (BSN)*. 377–382. https://doi.org/10.1109/BSN.2016.7516291

[44] G Ligorio, D Zanotto, A M Sabatini, and S K Agrawal. 2017. A novel functional calibration method for real-time elbow joint angles estimation with magnetic-inertial sensors. *Journal of Biomechanics* 54 (March 2017), 106–110.

[45] Xiaoyou Lin and Boon-Chong Seet. 2015. A Linear Wide-Range Textile Pressure Sensor Integrally Embedded in Regular Fabric. 15, 10 (Aug. 2015), 5384–5385.

[46] F Lorussi, E P Scilingo, A Tesconi, A Tognetti, and D De Rossi. [n. d.]. Wearable sensing garment for posture detection, rehabilitation and tele-medicine. In *International Conference on Information Technology - Applications in Biomedicine*. IEEE, 287–290.

[47] Roanna Lun and Wenbing Zhao. 2015. A Survey of Applications and Human Motion Recognition with Microsoft Kinect. *International Journal of Pattern Recognition and Artificial Intelligence* 29, 05 (2015), 1555008. https://doi.org/10.1142/S0218001415550083 arXiv:https://doi.org/10.1142/S0218001415550083

[48] Robert A. Malinzak, Scott M. Colby, Donald T. Kirkendall, Bing Yu, and William E. Garrett. 2001. A comparison of knee joint motion patterns between men and women in selected athletic tasks. *Clinical Biomechanics* 16, 5 (2001), 438 – 445. https://doi.org/10.1016/S0268-0033(01)00019-5

[49] Corinne Mattmann, Oliver Amft, Holger Harms, Gerhard Tröster, and Frank Clemens. 2007. Recognizing Upper Body Postures using Textile Strain Sensors. *ISWC* (2007), 1–8.

[50] Y Mengüç and Y L Park. 2013. Soft wearable motion sensing suit for lower limb biomechanics measurements. ... *(ICRA)* (2013).

[51] Pierre Merriaux, Yohan Dupuis, Rémi Boutteau, Pascal Vasseur, and Xavier Savatier. 2017. A Study of Vicon System Positioning Performance. *Sensors* 17, 7 (2017). https://doi.org/10.3390/s17071591

[52] Sebastian Münzner, Philip Schmidt, Attila Reiss, Michael Hanselmann, Rainer Stiefelhagen, and Robert Dürichen. 2017. CNN-based sensor fusion techniques for multimodal human activity recognition. *ISWC* (2017).

[53] W M Murray, S L Delp, TS Buchanan Journal of biomechanics, and 1995. [n. d.]. Variation of muscle moment arms with elbow and forearm position. *jbiomech.com* ([n. d.]).

[54] A. Nakamura, S. Tabata, T. Ueda, S. Kiyofuji, and Y. Kuno. 2005. Dance training system with active vibro-devices and a mobile image display. In *2005 IEEE/RSJ International Conference on Intelligent Robots and Systems*. 3075–3080. https://doi.org/10.1109/IROS.2005.1545565

[55] Michiro Negishi, Mark Abildgaard, Ilan Laufer, Terry Nixon, and Robert Todd Constable. 2008. An EEG (electroencephalogram) recording system with carbon wire electrodes for simultaneous EEG-fMRI (functional magnetic resonance imaging) recording. *Journal of Neuroscience Methods* 173, 1 (Aug. 2008), 99–107.

[56] N Obaid, M T Kortschot, M Sain Materials, and 2017. [n. d.]. Understanding the stress relaxation behavior of polymers reinforced with short elastic fibers. *mdpi.com* ([n. d.]).

[57] Kyung Wha Oh, Hyun Jin Park, and Seong Hun Kim. 2003. Stretchable conductive fabric for electrotherapy. *Journal of Applied Polymer Science* 88, 5 (May 2003), 1225–1229.

[58] Patrick Parzer, Adwait Sharma, Anita Vogl, Jürgen Steimle, Alex Olwal, and Michael Haller. 2017. SmartSleeve - Real-time Sensing of Surface and Deformation Gestures on Flexible, Interactive Textiles, using a Hybrid Gesture Detection Pipeline. *UIST* (2017), 565–577.

[59] Zhi-Tao Rao, Feng Yuan, Bing Li, and Ning Ma. 2014. Effect of elbow flexion angles on stress distribution of the proximal ulnar and radius bones under a vertical load: measurement using resistance strain gauges. *Journal of Orthopaedic Surgery and Research* 9, 1 (July 2014), 1–7.

[60] Jung-Sim Roh, Yotam Mann, Adrian Freed, and David Wessel. 2011. Robust and Reliable Fabric, Piezoresistive Multitouch Sensing Surfaces for Musical Controllers. *NIME* (2011).

[61] O Röhrle, M Sprenger, and S Schmitt. 2016. A two-muscle, continuum-mechanical forward simulation of the upper limb. *Biomechanics and Modeling in Mechanobiology* 16, 3 (Nov. 2016), 743–762.

[62] Stefan Schneegass and Alexandra Voit. 2016. GestureSleeve - using touch sensitive fabrics for gestural input on the forearm for controlling smartwatches. *ISWC* (2016).

[63] M Sergio, N Manaresi, F Campi, R Canegallo, M Tartagni, and R Guerrieri. 2003. A dynamically reconfigurable monolithic cmos pressure sensor for smart fabric. *IEEE Journal of Solid-State Circuits* 38, 6 (June 2003), 966–975.

[64] Shayan Seyedin, Joselito M Razal, Peter C Innis, Ali Jeiranikhameneh, Stephen Beirne, and Gordon G Wallace. 2015. Knitted Strain Sensor Textiles of Highly Conductive All-Polymeric Fibers. *ACS Applied Materials & Interfaces* 7, 38 (Sept. 2015), 21150–21158.

[65] Tien-Wei Shyr, Jing-Wen Shie, Chang-Han Jiang, and Jung-Jen Li. 2014. A Textile-Based Wearable Sensing Device Designed for Monitoring the Flexion Angle of Elbow and Knee Movements. *Sensors* 14, 3 (March 2014), 4050–4059.

[66] Hloniphile M Sithole, Sabyasachi Mondal, Precious Sibanda, and Sandile S Motsa. 2017. An unsteady MHD Maxwell nanofluid flow with convective boundary conditions using spectral local linearization method. *Open Physics* 15, 1 (Oct. 2017), 637–646.

[67] S Šlajpah, R Kamnik, and M Munih. 2014. Kinematics based sensory fusion for wearable motion assessment in human walking. *Computer Methods and Programs in Biomedicine* 116, 2 (Sept. 2014), 131–144.

[68] A. Soga, B. Umino, and M. Hirayama. 2009. Automatic Composition for Contemporary Dance Using 3D Motion Clips: Experiment on Dance Training and System Evaluation. In *2009 International Conference on CyberWorlds*. 171–176. https://doi.org/10.1109/CW.2009.37

[69] sorbothane.com. 2018. Hinge Joint. http://www.innerbody.com/image_skel07/skel31.html

[70] sparkfun. 2018. NW170-PI-20. PDF. https://cdn.sparkfun.com/datasheets/E-Textiles/Materials/NW170-PI-20%20TDS.pdf

[71] sparkfun. 2018. NW170-SLPA-2k. PDF. https://cdn.sparkfun.com/datasheets/E-Textiles/Materials/NW170-SLPA-2k%20TDS.pdf

[72] sparkfun. 2018. Velostat. PDF. https://cdn.sparkfun.com/datasheets/E-Textiles/Materials/NW170-PI-20%20TDS.pdf

[73] Seiichi Takamatsu, Takahiro Yamashita, and Toshihiro Itoh. 2016. Meter-scale large-area capacitive pressure sensors with fabric with stripe electrodes of conductive polymer-coated fibers. *Microsystem Technologies* 22, 3 (Feb. 2016), 451–457.

[74] Xiaoming Tao. 2005. Wearable eletronics and photonics. Elsevier.

[75] Alessandro Tognetti, Federico Lorussi, Nicola Carbonaro, and Danilo de Rossi. 2015. Wearable Goniometer and Accelerometer Sensory Fusion for Knee Joint Angle Measurement in Daily Life. *Sensors* 15, 11 (Nov. 2015), 28435–28455.

[76] Takanori Uchiyama, Tomoyuki Bessho, and Kenzo Akazawa. 1998. Static torque–angle relation of human elbow joint estimated with artificial neural network technique. *Journal of Biomechanics* 31, 6 (1998), 545–554.

[77] E J Van Zuylen, A van Velzen, and J J Denier van der Gon. 1988. A biomechanical model for flexion torques of human arm muscles as a function of elbow angle. *Journal of Biomechanics* 21, 3 (Jan. 1988), 183–190.

[78] Anita Vogl, Patrick Parzer, Teo Babic, Joanne Leong, Alex Olwal, and Michael Haller. 2017. StretchEBand - Enabling Fabric-based Interactions through Rapid Fabrication of Textile Stretch Sensors. *CHI* (2017).

[79] Sylvie Charlotte Frieda Anneliese von Werder and Catherine Disselhorst-Klug. 2016. The role of biceps brachii and brachioradialis for the control of elbow flexion and extension movements. *Journal of Electromyography and Kinesiology* 28, C (June 2016), 67–75.

[80] Junpu Wang, Pu Xue, Xiaoming Tao, and Tongxi Yu. 2013. Strain Sensing Behavior and Its Mechanisms of Electrically Conductive PPy-Coated Fabric. *Advanced Engineering Materials* 16, 5 (2013), 565–570.

[81] Zehong Wang, Wei Wang, and Dan Yu. 2017. Pressure responsive PET fabrics via constructing conductive wrinkles at room temperature. *Chemical Engineering Journal* 330 (Dec. 2017), 146–156.

[82] I Wicaksono. 2016. Design and Implementation of Multi-sensory Fabric as Deformable Musical Interface. (2016).

[83] Wikipedia. 2018. Gaussian Kernel Smoother. https://en.wikipedia.org/wiki/Kernel_smoother

[84] Wikipedia. 2018. Standard Linear Solid Model. https://en.wikipedia.org/wiki/Standard_linear_solid_model#Kelvin_representation

[85] Kevin E. Wilk, Michael M. Reinold, and James R. Andrews. 2004. Rehabilitation of the thrower's elbow. *Clinics in Sports Medicine* 23, 4 (2019/01/27 2004), 765–801. https://doi.org/10.1016/j.csm.2004.06.006

[86] M. B. Wilk and R. Gnanadesikan. 1968. Probability Plotting Methods for the Analysis of Data. *Biometrika* 55, 1 (1968), 1–17. http://www.jstor.org/stable/2334448

[87] www.nurbsfactor.com. 2018. Vicon Camera. http://www.nurbsfactor.com/hardware_vicon.php

[88] A Yao and M Soleimani. 2012. A pressure mapping imaging device based on electrical impedance tomography of conductive fabrics. 32, 4 (Sept. 2012), 310–317.
[89] Hui Zhang, Xiaoming Tao, Shanyuan Wang, and Tongxi Yu. 2016. Electro-Mechanical Properties of Knitted Fabric Made From Conductive Multi-Filament Yarn Under Unidirectional Extension. *Textile Research Journal* 75, 8 (July 2016), 598–606.
[90] Wu Zhou, Peng Peng, Huijun Yu, Bei Peng, and Xiaoping He. 2017. Material Viscoelasticity-Induced Drift of Micro-Accelerometers. *Materials* 10, 9 (2017), 1077.
[91] R Zhu and Z Zhou. 2004. A Real-Time Articulated Human Motion Tracking Using Tri-Axis Inertial/Magnetic Sensors Package. *IEEE Transactions on Neural Systems and Rehabilitation Engineering* 12, 2 (June 2004), 295–302.
[92] Matthias A Zumstein, Alexander Bürki, Anne-Sophie Massy, Philippe Zysset, and Beat K Moor. 2015. Extra-articular step osteotomy of the olecranon: A biomechanical assessment. *Clinical Biomechanics* 30, 10 (Dec. 2015), 1043–1048.

Received August 2018; revised December 2018; accepted January 2019